

Gravitational waves and nonaxisymmetric oscillation modes in mergers of compact object binaries

Nikolaos Stergioulas¹, Andreas Bauswein², Kimon Zagkouris¹ and Hans-Thomas Janka²

¹*Department of Physics, Section of Astrophysics, Astronomy and Mechanics Aristotle, University of Thessaloniki, Thessaloniki, 54124 Greece*

²*Max-Planck-Institut für Astrophysik, Karl-Schwarzschild-Str. 1, D-85748 Garching, Germany*

ABSTRACT

We study the excitation of nonaxisymmetric modes in the post-merger phase of binary compact object mergers and the associated gravitational wave emission. Our analysis is based on general-relativistic simulations, in the spatial conformal flatness approximation, using smoothed-particle-hydrodynamics for the evolution of matter, and we use a set of equal and unequal mass models, described by two nonzero-temperature hadronic equations of state and by one strange star equation of state. Through Fourier transforms of the evolution of matter variables, we can identify a number of oscillation modes, as well as several nonlinear components (combination frequencies). We focus on the dominant $m = 2$ mode, which forms a triplet with two nonlinear components that are the result of coupling to the quasiradial mode. A corresponding triplet of frequencies is identified in the gravitational wave spectrum, when the individual masses of the compact objects are in the most likely range of 1.2 to 1.35 M_{\odot} . We can thus associate, through direct analysis of the dynamics of the fluid, a specific frequency peak in the gravitational wave spectrum with the nonlinear component resulting from the difference between the $m = 2$ mode and the quasi-radial mode. Once such observations become available, both the $m = 2$ and quasiradial mode frequencies could be extracted, allowing for the application of gravitational-wave asteroseismology to the post-merger remnant and leading to tight constraints on the equation of state of high-density matter.

Key words:

1 INTRODUCTION

Mergers of binary compact objects are prime sources for second- and third-generation interferometric gravitational wave (GW) detectors (Abbott et al. 2009; Acernese et al. 2006; Abadie et al. 2010). The expected GW signals from such events are estimated through general-relativistic hydrodynamical simulations (see Duez 2010 for a review). The outcome of these simulations depends on the binary parameters and on the equation of state (EOS) of high-density matter. The latter is rather uncertain (Lattimer & Prakash 2007; Steiner et al. 2010) and currently it is unclear whether, for a given binary mass, the merger would lead to a hypermassive compact object or to prompt collapse to a black hole. If a hypermassive compact object forms, it will not be axisymmetric, but it will show transient nonaxisymmetric deformations, such as a bar-like shape, spiral arms, a double core structure and quasiradial and nonaxisymmetric oscillations of the matter. Strong nonaxisymmetric features should be distinguishable in the GW signal and could be used for characterizing the hypermassive compact object (Zhuge et al. 1994; Oechslin et al. 2002; Shibata & Uryū 2002; Shibata et al. 2005; Shibata & Taniguchi 2006; Oechslin & Janka 2007; Baiotti et al. 2008; Kiuchi et al. 2009; Bauswein et al. 2010).

Here, we analyze the formed hypermassive compact object as an isolated gravitating fluid, studying its oscillation modes. Fourier

transforms of the evolved variables reveal that the fluid is oscillating in a number of modes that have discrete frequencies throughout the star. Furthermore, we also identify several nonlinear components, sums and differences of discrete oscillation modes. The oscillations identified in the fluid are in direct correspondence with peaks in the GW spectrum, as obtained through the quadrupole formula. We focus on the main quadrupole ($m = 2$) oscillation mode of the fluid, which appears as a triplet, the side bands being due to the nonlinear coupling to the fundamental quasiradial ($m = 0$) mode. The lowest-frequency side band, the difference between the $m = 2$ and $m = 0$ frequencies, coincides with a peak in the GW spectrum that characterizes the merger phase in all models, in which the mass of both compact objects are in the range of 1.2 to 1.35 M_{\odot} . We thus propose that in the event of detection, one could extract both the $m = 0$ and $m = 2$ mode frequencies of the merged object, which could lead to tight constraints on the EOS of high-density matter. In effect, such a detection would enable an analysis with GW asteroseismology of the remnants of binary compact object mergers.

The simulation code is based on general relativistic smoothed-particle-hydrodynamics (SPH) and on a spatially-conformally-flat spacetime approximation, as described in detail in Bauswein et al. (2010) and references therein. We simulate the merger of the compact objects following the evolution from the late inspiral phase

through the merging and the formation of the hypermassive remnant, until a quasi-stationary state is reached.

The paper is structured as follows: In Sec. 2 we discuss the initial data used in our simulations. In Sec. 3 we outline the numerical methods used in the simulations and in the mode extraction procedure. Section 4 presents our results in detail, while in Sec. 5 we compare them to previous results in the literature. We conclude with Sec. 6.

2 INITIAL DATA

We consider two different models of hadronic EOSs, referred to as Shen (Shen et al. 1998) and LS (Lattimer & Swesty 1991) and a strange quark matter EOS, referred to as MIT60. Since during merging temperatures of more than several ten MeV can be reached, all three EOSs take into account non-zero temperature effects (see Bauswein et al. 2010 for a discussion of the importance of temperature effects in the merger context).

The Shen EOS was derived within a relativistic mean-field theory and assumes an incompressibility modulus for nuclear matter of $K = 280$ MeV (Shen et al. 1998). Solving the relativistic equations of hydrostatic equilibrium, nonrotating neutron stars described by the Shen EOS have radii of about 15 km in the mass range of 0.5 to 1.7 M_{\odot} . The maximum mass of nonrotating stars is 2.2 M_{\odot} . For the LS EOS a liquid-drop model with $K = 180$ MeV was adopted (Lattimer & Swesty 1991), which yields neutron stars more compact in comparison to the Shen EOS. Typical radii are of the order of 12 km for masses of 0.5 to 1.6 M_{\odot} . The LS EOS supports nonrotating objects with masses slightly above 1.8 M_{\odot} .

The MIT60 EOS follows from the strange matter hypothesis (Bodmer 1971; Witten 1984), i.e. that 3-flavor quark matter of up, down and strange quarks is more stable than ordinary nuclear matter. In such a case, compact stars would be strange stars rather than neutron stars (see e.g. Glendenning 1996; Haensel et al. 2007), which has not been strictly ruled out theoretically or observationally at this point. For the MIT60 EOS the MIT Bag model (Farhi & Jaffe 1984) was employed, with a bag constant of 60 MeV/fm³ (see Bauswein et al. 2010 for details). Strange star models are generally more compact than neutron star models of the same mass. Furthermore, the mass-radius relation of strange stars does not show the typical inverse relation of neutron stars. The mass-radius relation for all three EOSs included in our study can be found in Fig. 2 of Bauswein et al. (2010).

We note that the recent discovery of a 2 M_{\odot} pulsar (Demorest et al. 2010) practically rules out EOSs which yield maximum masses of nonrotating compact stars below this limit. The maximum masses of nonrotating stars for the LS and MIT60 EOSs employed here fall short of this requirement, but not dramatically. Though to date several finite-temperature EOSs (Typel et al. 2010; Hempel & Schaffner-Bielich 2010; Shen et al. 2010a,b, 2011; Shen et al. 2011) have been published, at the time of writing only those introduced above have been available to us and successfully incorporated in the simulation code. Thus, leaving out the LS and MIT60 EOSs would leave us with a single EOS, which would not test the sensitivity of our results to the choice of EOS. We thus include the LS and MIT60 EOSs in our study for the sole purpose of estimating the sensitivity of our conclusions to the EOS employed, keeping in mind their disadvantage. Nevertheless, the individual stars that make up the binaries have masses significantly lower than the maximum mass limit, and the hypermassive object formed as a result of the merger is supported against col-

lapse by strong differential rotation. Because of this, the outcome of the simulations with the LS and MIT60 EOSs is still useful for qualitative comparisons to the cases where the Shen EOS is used.

The masses of compact stars in binaries cluster at about 1.35 M_{\odot} (Thorsett & Chakrabarty 1999; Zhang et al. 2010), which is also predicted by population synthesis studies (e.g. Belczynski et al. 2008). Therefore, we focus in our analysis on systems with two neutron stars with a gravitational mass of 1.35 M_{\odot} . In order to investigate unequal-mass mergers, we also consider configurations with a 1.2 M_{\odot} neutron star and a more massive companion of 1.35 M_{\odot} . For the MIT60 EOS, we include a configuration with two low-mass stars of 1.1 M_{\odot} each, an unequal-mass binary with 1.2 M_{\odot} and 1.35 M_{\odot} , and a configuration with two stars of 1.35 M_{\odot} each. In the latter case, however, the hypermassive object formed after merging only survives for a few dynamical timescales before collapsing to a black hole, and we do not discuss this model in our study. Table 1 lists all models considered further, where, for example, Shen 12135 refers to the simulation with a 1.2 M_{\odot} and a 1.35 M_{\odot} star employing the Shen EOS.

3 NUMERICAL METHODS

3.1 Simulations

The hydrodynamical simulations of the binary merger and the post-merger remnant are performed with a three-dimensional general-relativistic SPH code. The Einstein field equations are solved within the condition of spatial conformal flatness, which requires the additional implementation of a GW backreaction scheme. For details of the code see Oechslin et al. (2002, 2007). The calculations start from a quasi-equilibrium orbit about three revolutions before the actual merger. For the neutron star models about 500,000 SPH particles are used, while the flat density profile of strange stars allows for a lower SPH particle resolution of about 130,000 particles. Simulations with a somewhat higher number of particles do not significantly affect the main features of our results. The simulations are carried out until a stable remnant in approximate rotational equilibrium has formed and oscillates for tens of dynamical timescales, or until the delayed collapse to a black hole occurs.

The dynamics of the models used in this study have been extensively discussed in Bauswein et al. (2010), and the reader is referred to this publication for details. Here we only give a brief outline: While orbiting around the common center of mass, the stars approach each other increasingly faster due to angular momentum and energy losses by the GW emission. Prior to merging, tidal forces start to deform the stars. The strength of this effect depends on the EOS and on the masses of the binary components. The deformation is pronounced for the Shen EOS, but relatively small for the strange star models. Finally, the stars merge into a rotating double-core structure, where the two dense cores appear to bounce against each other a few times to ultimately form a differentially rotating hypermassive object with a single core. In the case of unequal masses, such as our models Shen 12135 and LS 12135, the less massive binary component is tidally stretched and wrapped around the more massive one. Moreover, an extended spiral arm develops, feeding a dilute halo around the differentially rotating central object. In the case of the unequal mass strange star model MIT60 12135, the outcome is more similar to the equal mass case, because of the reduced tidal effects.

The equal-mass neutron star mergers also form thick disks around the remnants, because matter is shed off from the whole

surface of the hypermassive objects. In contrast, the remnants of merging strange stars terminate at a sharp surface, as did the initial stars. Matter is stripped off only later in the evolution when angular momentum transfer leads to the formation of two thin spiral arms, which then form a fragmented thin disk around the central object.

The hypermassive remnants of the merger are supported against gravitational collapse by differential rotation and thermal pressure. However, ongoing angular momentum transfer and loss by mass shedding finally leads to gravitational collapse and black hole formation. The delayed collapse can take up to hundreds of milliseconds for low-mass models, but our simulations were terminated at about 10 to 20 ms after merging.

The GW emission of our models is analyzed by means of the quadrupole formula. In the low-frequency regime the spectra are not reliable because we simulate only a small fraction of the inspiral phase and thus miss most of the low-frequency part of the signal.

3.2 Mode Extraction

The original simulation data in different two-dimensional planes are first mapped onto a Cartesian grid of size $n_x \times n_y = 51 \times 51$. We then perform Fourier analysis of evolved variables over the whole grid (but focusing mainly on the equatorial plane) and identify the predominantly excited modes, which appear as discrete frequencies in the Fourier spectrum. At selected mode frequencies, we proceed with extracting the shape of the mode eigenfunctions, using a method described in Stergioulas et al. (2004). The two-dimensional shape of the eigenfunction in the equatorial plane correlates directly with the amplitude of the Fourier transform at a given mode frequency. At nodal lines, care must be taken to switch the sign of the eigenfunction. This method was first applied in Stergioulas et al. (2004) to the case of axisymmetric modes, where two-dimensional eigenfunctions were extracted in a plane that passes through the rotational axis. Here, we find that the same method can be used for extracting the eigenfunctions of non-axisymmetric modes in the equatorial plane. We note that for all modes that were identified, the mode frequency was discrete throughout the star and identical in all hydrodynamical variables.

To our knowledge, this is the first direct demonstration that once a hypermassive object forms after a binary merger, it behaves as an isolated, self-gravitating system and its dynamics can be described as a superposition of different oscillation modes (in a differentially rotating background). Departures from a background equilibrium state can be described (up to a certain degree) by nonlinear features of the oscillations. We note that the background is varying in time, so that individual frequency peaks are broadened. Nevertheless, the frequency peaks remain sufficiently narrow to identify individual modes.

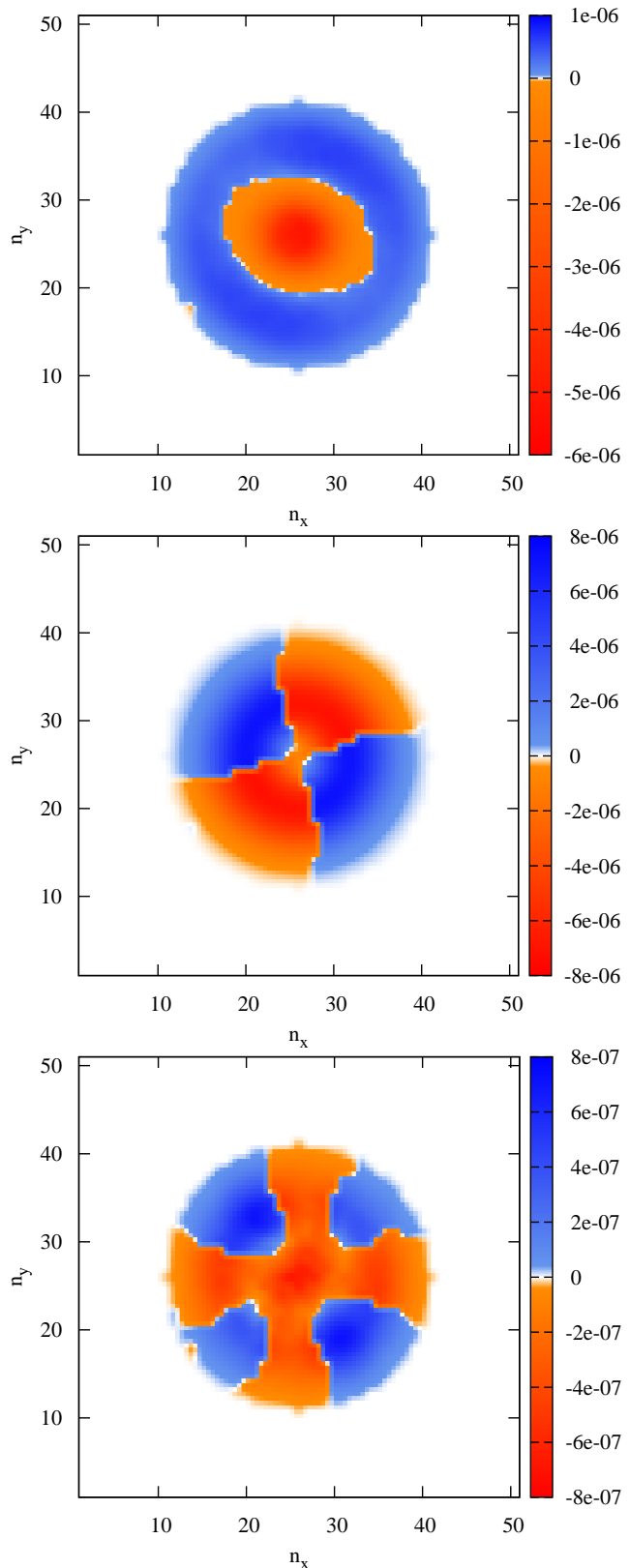


Figure 1. Projection in the equatorial plane of the extracted $m = 0, 2$ and 4 mode eigenfunctions (from top to bottom) for the oscillations in pressure of model Shen 135135. The two axes count individual grid points of the Cartesian grid used for the mode analysis. The color scale only has a relative meaning.

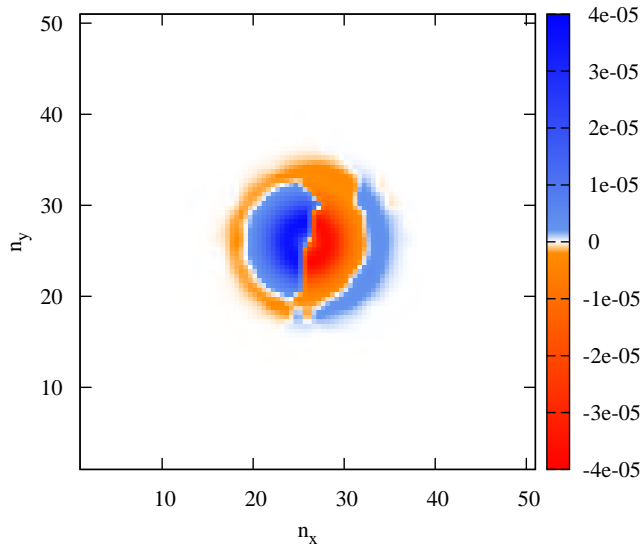


Figure 2. Projection in the equatorial plane of the extracted $m = 1$ mode eigenfunction, for the oscillations in pressure of model MIT60 12135.

4 RESULTS

4.1 Two-dimensional eigenfunctions

Non-isentropic, differentially rotating, compact objects can oscillate in a large number of different quasinormal modes, (f -modes, p -modes, g -modes and inertial modes, distinguished by three different mode numbers, l , m and n , the latter one being the radial order, see Stergioulas (2003) for a review). Here, we only characterize the structure of the extracted modes in the equatorial plane, in terms of the mode number m . A complete characterization and identification with specific quasinormal modes would require a much more detailed analysis that is out of the scope of the current work. In particular, neither a linear, nor a nonlinear complete analysis of possible oscillation modes has been done for remnants of mergers of compact objects, to date, with which we could directly compare our results. As such, we will talk about “modes” and “eigenfunctions” even though we have not strictly shown a correspondence to specific linear quasinormal modes. Nevertheless, for the purpose of explaining the main observable features of GWs from nonaxisymmetric oscillations in binary compact object mergers, our present approach suffices.

In the Fourier transform of hydrodynamical variables, the dominant mode is always the $m = 2$ mode. For equal-mass mergers, the even mode numbers are predominantly excited, while for unequal-mass mergers, the odd mode numbers are also considerably excited (mainly the $m = 1$ mode). The modes can be identified by inspection of the extracted two-dimensional eigenfunction in the equatorial plane. Representative cases are shown in Figs. 1 and 2, which display the eigenfunctions (in pressure oscillations) of the $m = 0$, 2 and 4 modes for the equal-mass model Shen 135135 and the $m = 1$ mode for the unequal-mass model MIT60 12135. The $m = 0$ (quasiradial) eigenfunction is dominated by a spherically symmetric contribution, while an additional, small (rotationally-induced) quadrupole distortion is also present. As expected for this type of eigenfunction, there is a nearly circular nodal line in the pressure perturbations, characteristic of the fundamental radial mode.

The eigenfunction of the $m = 2$ mode shows a very sharp quadrupole pattern, induced by the merger of the two individual

stars. The two nodal lines are, as expected, nearly perpendicular to each other. The $m = 4$ mode eigenfunction shows a characteristic octupole pattern. The alternating regions are of nearly the same size, but due to the very low amplitude of excitation and the finite duration of the time-series, the Fourier transform also picks up a non-zero contribution at the center of the star, which means that for this mode we are approaching the accuracy of our method. Higher-order modes should also be excited (and there are indeed a large number of peaks in the Fourier transform at high frequencies) but their amplitude is so small that any extracted eigenfunction will be dominated by numerical errors.

Fig. 2 shows the eigenfunction of the $m = 1$ mode excited during the merger of the unequal-mass model MIT60 12135. A nodal line that cuts through the center of the star is characteristic of this mode. Notice that conservation of momentum prohibits the existence of a fundamental $m = 1$ mode, as this would induce a linear motion of the center of mass. However, higher-order overtones are allowed, so the extracted mode should be identified as the (lowest-frequency) first overtone of the $m = 1$ modes. This is supported by the additional, nearly circular node line, which allows for momentum conservation during the oscillation.

4.2 Mode frequencies

Table 1 lists the extracted mode frequencies (in the inertial frame, defined by coordinate time t) for the various models. We note that the frequencies of the quasiradial ($m = 0$) mode differ significantly among the three chosen EOSs. In the selected mass-range, this frequency is lowest for the Shen EOS (about 0.5kHz). It doubles to about 1kHz for the LS EOS and it reaches up to about 1.5kHz for the MIT60 EOS. This mode frequency is affected mainly by two factors: the compactness of the star and the distance of the model from the region of axisymmetric instability to collapse. At the boundary of this region, the frequency of the quasiradial mode goes through zero. On the other hand, higher compactness leads to higher mode-frequency. But, because of the axisymmetric instability, the quasiradial mode frequency can be small for any EOS, as long as the model is near the instability threshold. This latter property explains the fact that, for each EOS, the models with larger total mass have smaller quasiradial mode frequency.

The frequency of the $m = 2$ mode depends mainly on the compactness of the star and for the models in Table 1 it is roughly 2 kHz for the stiffer Shen EOS and roughly 3kHz for the softer LS EOS and for the MIT60 EOS. As expected, for each EOS, it is higher for the more massive (hence more compact) model. In all unequal mass cases, we were able to extract the $m = 1$ mode frequency, which is induced by the unequal distribution of mass just prior to merging. The additional $m = 3$ mode was extracted for the Shen and LS EOSs, while in three models we could also identify the $m = 4$ mode.

A remarkable property of the nonaxisymmetric modes $m = 1...4$ is that the extracted frequencies are nearly integer multiples of the frequency of the $m = 1$ mode. This property holds true with good accuracy for the equal-mass cases, while for the unequal-mass mergers it is less accurate, but still roughly true.

4.3 A representative model

The evolution of the GW amplitude h_+ expected from the late binary inspiral, merger and post-merger phases for the unequal-mass model Shen 12135 is shown in the top panel of Fig. 3. The merger

Table 1. Extracted mode frequencies.

Model	$f_{m=0}$ (kHz)	$f_{m=1}$ (kHz)	$f_{m=2}$ (kHz)	$f_{m=3}$ (kHz)	$f_{m=4}$ (kHz)
Shen 12135	0.50	1.07	2.14	3.22	4.26
Shen 135135	0.46	–	2.24	–	4.11
LS 12135	1.10	1.55	3.12	4.66	–
LS 135135	0.98	–	3.30	–	–
MIT60 1111	1.56	–	2.92	–	5.94
MIT60 12135	1.24	1.72	3.26	–	–

takes place at around $t = 17$ ms from the start of the simulation. A characteristic sudden change in the frequency and phase of the waveform takes place at the onset of merging. After a few highly nonlinear oscillations, the waveform settles into a more regular pattern. The late-time damping of the waveform is the result of a combination of shock-induced dissipation of oscillations and numerical damping. Gravitational-wave damping is effective only on larger timescales than shown here. With less numerical damping, the gravitational wave amplitude could remain strong for a much longer time, leading to an enhanced signal (for a recent long-term evolution see Rezzolla et al. (2010)).

Irrespective of the true damping timescale, we are interested mainly in the frequency spectrum, which is shown in the middle panel of Fig. 3. We plot the scaled power spectral density, $h_+(f)\sqrt{f}$ (black curve), where $h_+(f)$ is the Fourier transform of $h_+(t)$, which is directly comparable with the anticipated sensitivity for Advanced LIGO presently being installed (Harry & the LIGO Scientific Collaboration (2010)) and the projected Einstein Telescope (ET) detectors (Punturo et al. (2010); Hild et al. (2010)) (dotted red and blue curves, respectively). Note that the sensitivity of the advanced Virgo detector (Acernese et al. (2006)) is planned to be similar to the one of the Advanced LIGO detector. Therefore, we include the latter only as an example for the class of detectors going into operation within the next years. The distance to the source is assumed to be 100 Mpc. We also show the same quantity during the pre-merger phase only (red curve) and during the post-merger phase only (green curve). The first peak at roughly 900Hz is artificial, because our simulations only start at a few orbits before merging, so most of the actual inspiral phase is missing. The largest peak (denoted by f_2) at about 2kHz is clearly produced exclusively in the post-merger remnant. In addition to this peak, which is very pronounced and clearly detectable by ET and with good prospects for detection by Advanced LIGO, there are two more characteristic peaks, denoted by f_- and f_+ , which are also produced in the post-merger phase and have good prospects for detection by ET (more so for f_- than for f_+). These two peaks are both above the ET noise curve and above the contribution of the pre-merger (inspiral) waveform to the FFT of the signal. There are additional peaks above the ET noise curve in the range of 1kHz to 1.5kHz, which, however, will be superseded by the inspiral signal, unless the post-merger signal is analyzed separately from the inspiral part. Furthermore, the high-frequency peaks that are below the ET noise curve will not concern us.

The three frequencies f_- , f_2 and f_+ form a triplet, which we will attempt to interpret in terms of the oscillation modes of the post-merger remnant. The bottom panel of Fig. 3 shows the amplitude of the Fourier transform of the evolution of the pressure along a fixed coordinate line in the equatorial plane which passes through the center of the coordinate system (this is an integrated amplitude, taking into account the contributions along the whole coordi-

nate line). The Fourier amplitude is composed of several very distinct and narrow peaks, which correspond to the discrete $m = 0, 1, 2, 3$ and 4 mode frequencies. In addition, a number of smaller peaks are seen. The latter are nonlinear components, combination frequencies of the main oscillation modes, i.e. linear sums and differences¹ (see Zanotti et al. (2005); Passamonti et al. (2007) and references therein). The difference of the frequencies of the $m = 2$ and $m = 0$ mode is denoted as “2-0”, their sum as “2+0” (and similarly for other components). A two-dimensional plot of the Fourier amplitude of the pressure evolution at the “2-0” frequency reveals that indeed it is a combination of a radial and a quadrupolar pattern.

By comparison of the middle and bottom panels of Fig. 3, there is an obvious near coincidence of the frequency peak f_2 in GWs with the frequency of the $m = 2$ mode of the post-merger remnant. Furthermore, the other two peaks of the GW triplet, f_- and f_+ , nearly coincide with the “2-0” and “2+0” combinations of the pressure oscillations. As we will see, this is a generic behaviour for all models (except for the very low mass MIT60 1111 model). It is thus tempting to attribute the f_- peak in the GW spectrum to a nonlinear interaction between the quadrupole and quasiradial modes. Essentially, a double core structure that appears and disappears several times in the early post-merger phase could be the result of (or could be described by) this nonlinear interaction. To firmly establish this goes beyond the scope of the present work, but already the coincidence of the f_- and “2-0” frequencies has practical consequences: it allows the determination of both the $m = 2$ and $m = 0$ oscillation frequencies of the post-merger remnant. In combination with the additional knowledge of the characteristics of the compact objects from the detection of the inspiral signal (see Read et al. (2009) and references therein), the determination of at least two independent oscillation frequencies should allow for the application of the theory of GW asteroseismology, placing very stringent constraints on several properties of the post-merger remnant and consequently on the EOS of high-density matter (for an application of GW asteroseismology to isolated, rotating neutron stars, see Gaertig & Kokkotas (2011)).

4.4 A survey of different models

Having examined in detail model Shen 12135 as a representative case, it is instructive to compare the main results to the equal-mass case Shen 135135 (Fig. 4). The GW spectrum (middle panel of Fig. 4) is very similar to the representative case, except for small differences in the frequencies of the main peaks. In the Fourier transform of the pressure evolution (bottom panel of Fig. 4), the odd modes $m = 1$ and 3 are no longer as strong as in the unequal-mass case, and the evolution is mainly determined by the $m = 2$ mode, while the $m = 0$ and $m = 4$ modes are also present and so are nonlinear components. Again, there is a coincidence between the frequency of the f_- peak in the GW spectrum and the “2-0” combination frequency in the pressure evolution.

The unequal-mass model LS 12135 shows similar qualitative properties as the corresponding Shen 12135 model, except that all mode frequencies are considerably higher. In addition, a larger number of nonlinear components can be clearly identified (bottom panel of Fig. 5). The f_- vs. “2-0” coincidence remains. The corresponding equal-mass model LS 135135 shows only the $m = 0$ and $m = 2$ modes dominating, with the addition of the “2-0” and

¹ These combination frequencies are also called bilinear coupling (or intermodulation) components.

“2+0” combination frequencies. As in the previous models, there is again an f_- vs. “2-0” coincidence.

For the strange matter EOS MIT60, we examined the equal-mass case MIT60 1111, where each individual component of the binary system has a mass of only $1.1 M_\odot$ (Fig. 7). The reason is that for an individual mass of $1.35 M_\odot$, an equal-mass binary system forms a black hole soon after merging. Notice that the density profile of the MIT60 models differs drastically from the case of the hadronic EOSs. It is very flat and terminates at a high value at the surface. Especially for the low-mass model of $1.1 M_\odot$, the density profile is roughly uniform. This causes the oscillation properties of the MIT60 models to differ considerably from those of the hadronic models. The GW spectrum of the MIT60 1111 model is still qualitatively similar to the previous hadronic models and one can still identify a triplet of frequencies f_- , f_2 and f_+ . However, in this case, the frequency of the quasiradial mode is higher than for the hadronic models and, in fact, coincides with the frequency of the “2-0” nonlinear component. The latter differs, for this model only, from the f_- peak in the GW spectrum. It is possible that the f_- , f_2 and f_+ triplet is caused by the nonlinear interaction of the f_2 mode with a mode other than the quasiradial mode or that these are combination frequencies of higher order. Notice also that, for this model, the frequency of the $m = 2$ mode is twice the frequency of the quasiradial mode. Such a coincidence, which leads to a resonance between the two modes and to enhanced GW emission has also been observed in simulations of phase-transition-induced instabilities in rotating compact stars (Abdikamalov et al. 2009; Dimmelmeier et al. 2009).

For the unequal mass MIT60 12135 model (Fig. 7), the frequency of the quasiradial mode is smaller than for the MIT60 1111 model, while the frequency of the $m = 2$ mode is higher. As a consequence, the frequency of the “2-0” nonlinear component is not far from the f_- peak in the GW spectrum, although the agreement is not as good as in the case of the hadronic EOSs. One should keep in mind, however, that the post-merger remnant is evolving in time, contracting its radius and reaching higher densities. This is causing the different oscillation frequencies to change continually in time. One cannot, therefore, expect a perfect match between the measured peaks in the Fourier transform of evolved variables and the nonlinear features of the GW spectrum.

We thus find that the GW spectrum of the post-merger phase is characterized by a triplet of frequencies that clearly coincides with the frequencies of the $m = 2$ oscillation mode of the fluid and its interaction with the quasiradial mode in all cases with mass in the range $1.2 M_\odot$ to $1.35 M_\odot$. Only in the low-mass MIT60 1111 case the triplet has a different origin.

5 COMPARISON TO PREVIOUS WORK

Allen et al. (1999) presented an initial study of binary neutron star mergers as a linear perturbation problem of an isolated star (a so-called close-limit approximation, in analogy to the corresponding approximation in binary black hole mergers). They showed that several fluid modes would be excited, but their study, being linear, did not take into account nonlinear combination frequencies, as we do here in our fully nonlinear approach.

In Zhuge et al. (1994) the frequency peak f_- in the GW spectrum was associated with the rotating barlike structure formed immediately after merging, while it was suggested that the main f_2 peak is due to a low-order p -mode. Oechslin et al. (2002) proposed that the f_2 peak, being the quadrupole frequency of the post-merger

remnant, could be used to distinguish a soft EOS from a stiff EOS. Shibata & Uryū (2002) also suggested that the post-merger GW spectrum is produced by non-axisymmetric oscillation modes of the merged object and arrived at empirical relations (for polytropic EOSs) for the two frequencies f_- and f_2 , without identifying their origin. Based on the dependence of these two frequencies on the parameters of the polytropic EOS, they suggested that these two frequencies could be used to constrain the stiffness of the EOS.

In Shibata et al. (2005) it was suggested that quasiradial oscillations modulate the post-merger signal and it was noticed that the difference in frequency between the two main peaks (i.e. the peaks we call f_- and f_2 here) is approximately equal to the frequency of the quasiradial oscillation. Furthermore, in Shibata & Taniguchi (2006) and in Kiuchi et al. (2009) two strong sideband peaks (forming a triplet with the f_2 peak) were pointed out to exist in some cases and were associated with a modulation by large-amplitude quasiradial oscillations. The results of our mode analysis are in line with the above observations and expectations.

In contrast, Baiotti et al. (2008) described the repeated appearance of a double core structure in a particular high-mass merged object as a dynamical bar-mode instability which develops and is quickly suppressed again several times. The double core structure appeared at a regular interval of 2 ms. According to our current results, this should be simply the period of the quasiradial oscillation and instead of a dynamical instability the modulation is due to the “2-0” nonlinear component (in other, low-mass models presented in Baiotti et al. (2008), a bar persists for a long time and a possible association to a dynamical instability is worth further investigation).

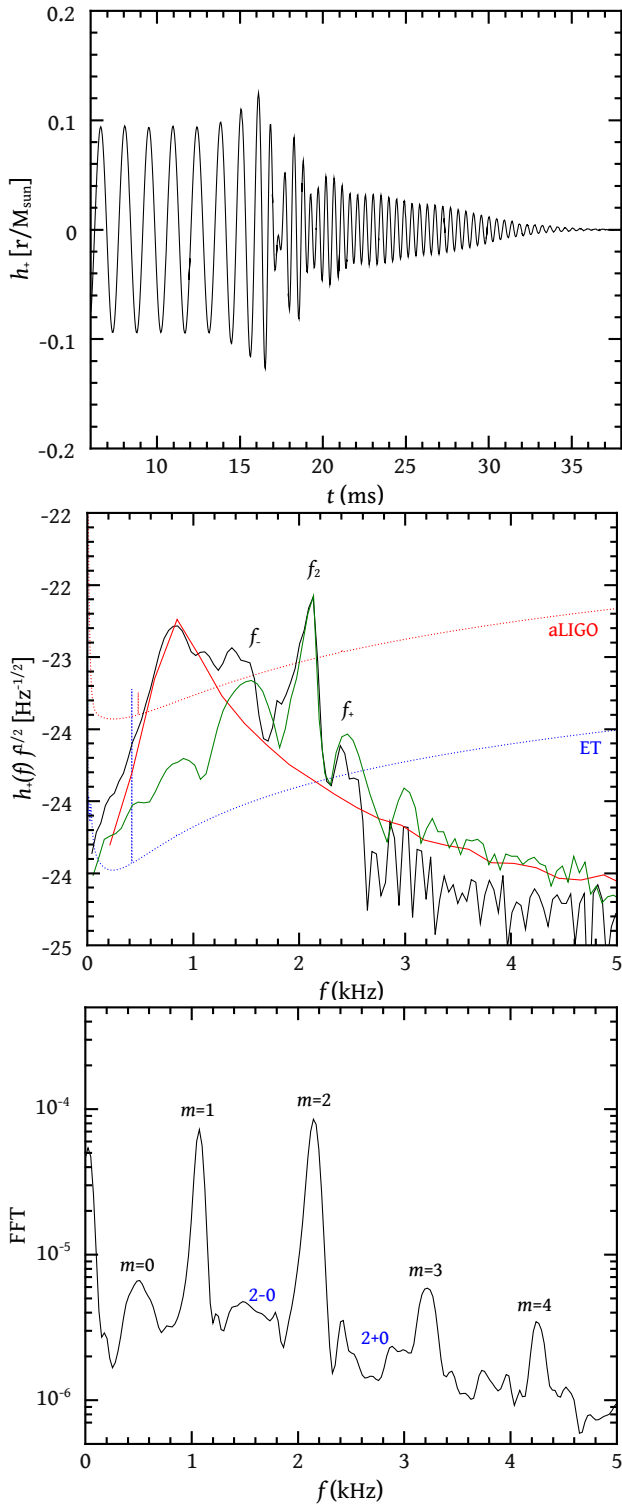


Figure 3. Model Shen 12135 – Top panel: Time evolution of the GW amplitude h_+ . Middle panel: Total (black), pre-merger (red) and post-merger (green) scaled power spectral density, compared to the Advanced LIGO and ET unity SNR sensitivity curves (Harry & the LIGO Scientific Collaboration (2010); Hild et al. (2010)). The distance to the source is assumed to be 100 Mpc. Bottom panel: Amplitude of FFT for the time evolution of the pressure, p , in the equatorial plane. Several oscillation modes, as well as nonlinear combination frequencies (blue labels) are identified.

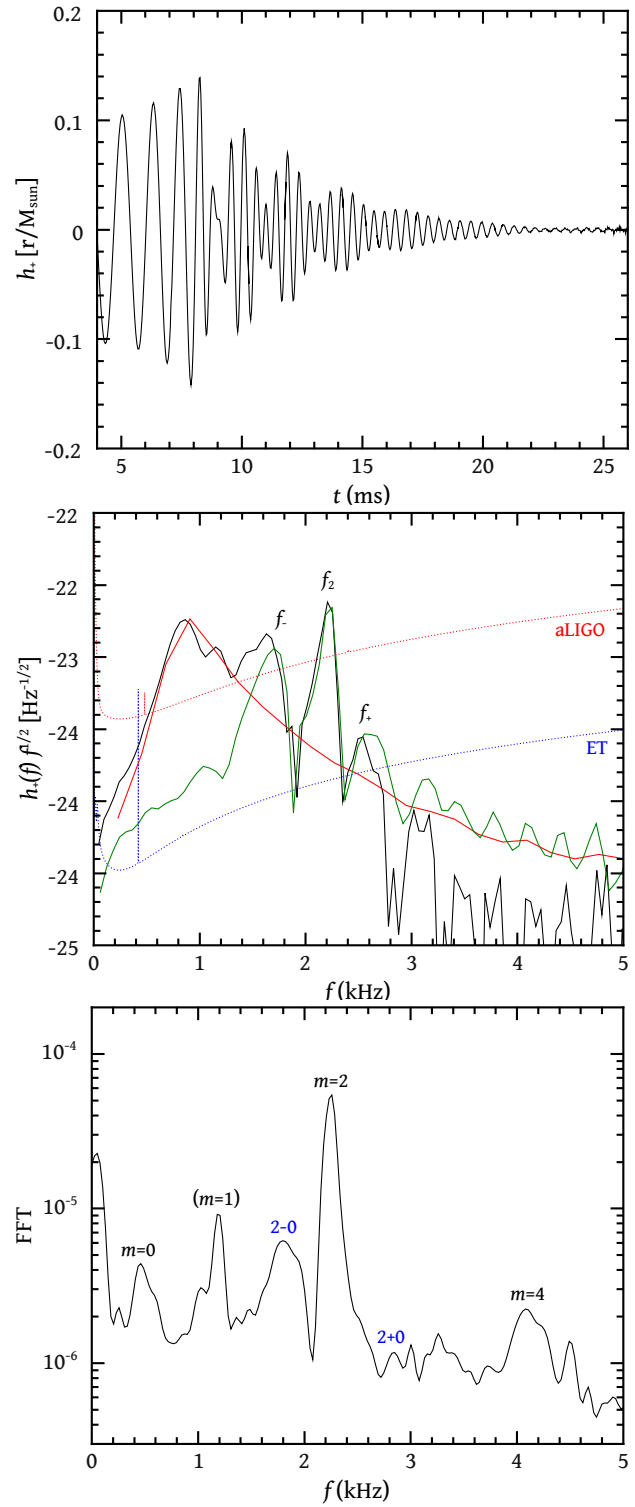


Figure 4. Same as Fig. 3, but for model Shen 135135.

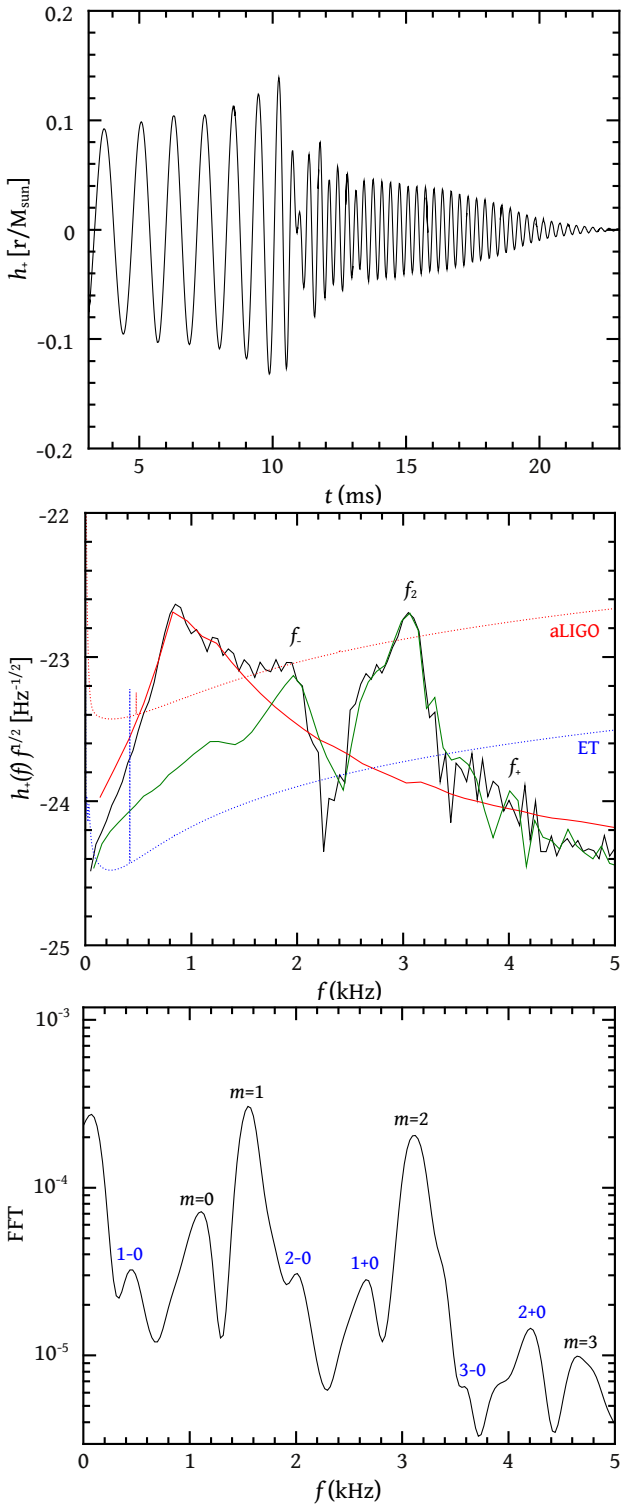


Figure 5. Same as Fig. 3, but for model LS 12135.

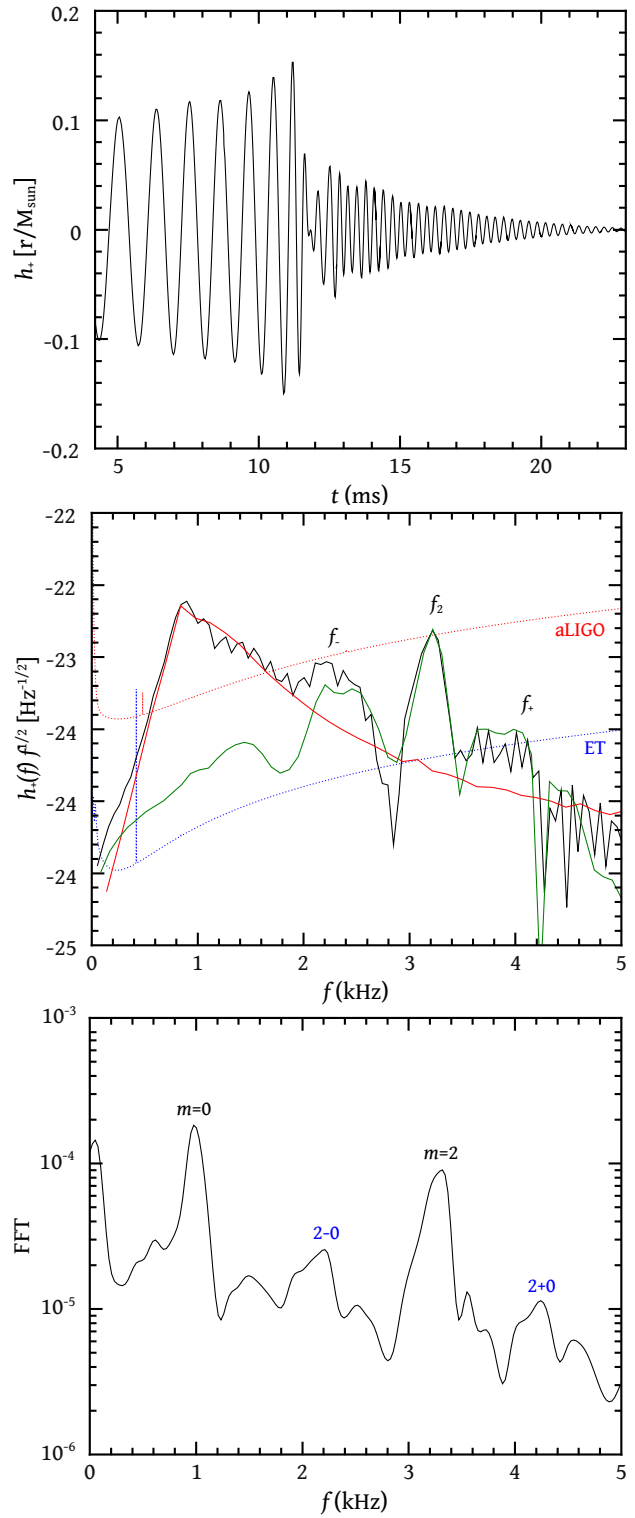


Figure 6. Same as Fig. 3, but for model LS 135135.

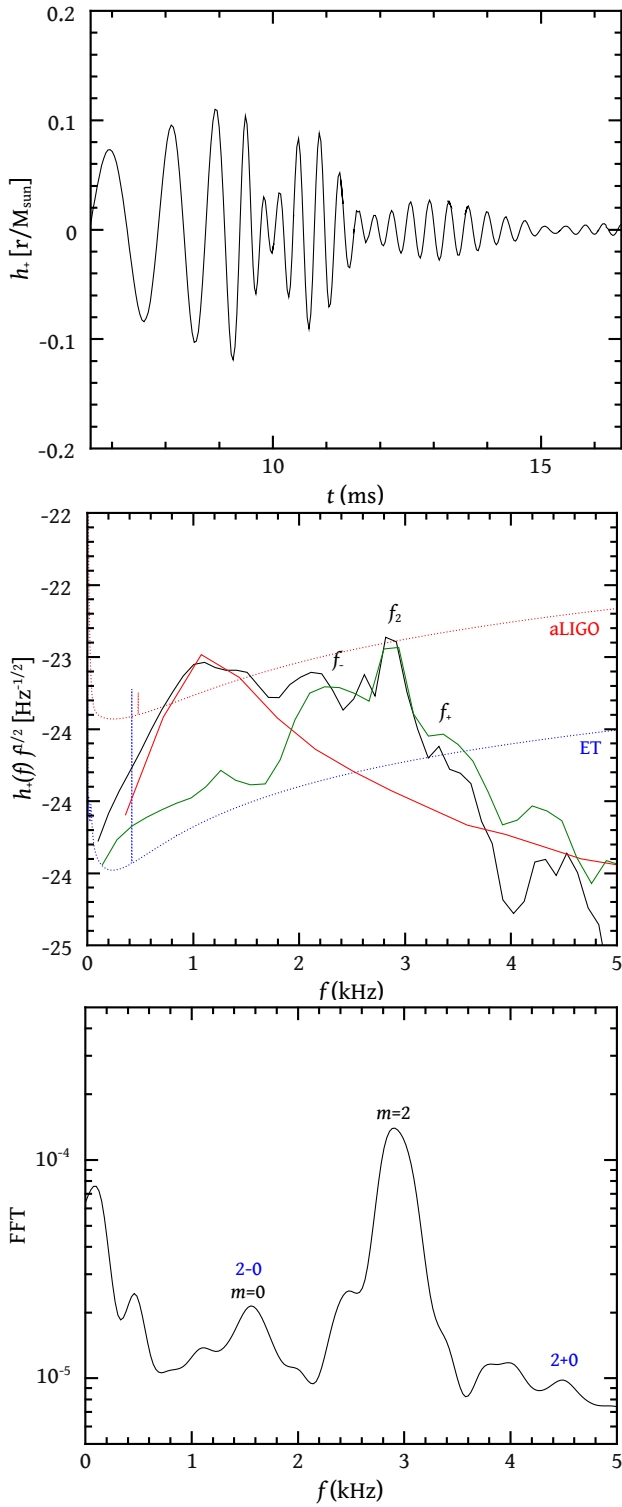


Figure 7. Same as Fig. 3, but for model MIT60 1111.

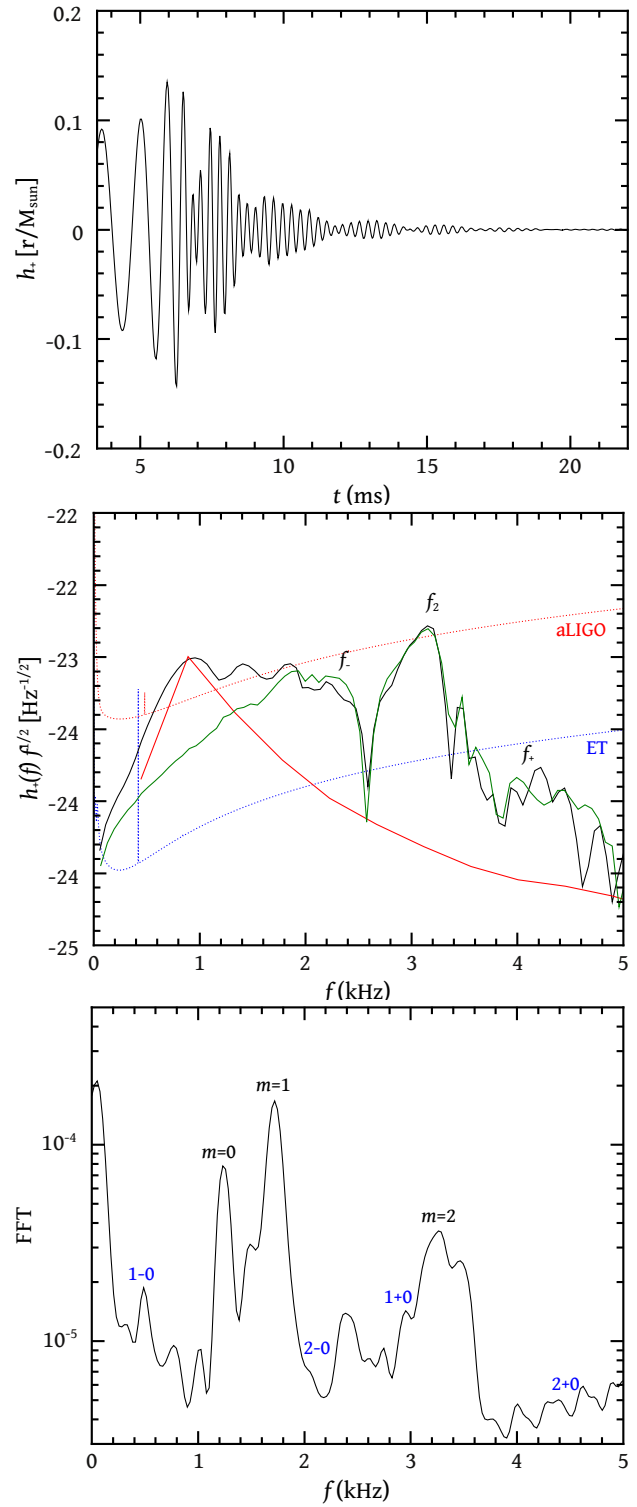


Figure 8. Same as Fig. 3, but for model MIT60 12135

6 CONCLUSIONS

We have studied the excitation of nonaxisymmetric oscillations in the post-merger phase of binary compact object mergers. Our analysis is based on general-relativistic simulations, using SPH for the evolution of matter, and we used a set of equal-mass and unequal-mass models, described by two nonzero-temperature hadronic EOSs and by one strange star EOS. We studied the oscillations through Fourier transforms of the evolved matter variables and identified a number of oscillation modes, as well as several nonlinear components (combination frequencies). The dominant $m = 2$ mode forms a triplet with two nonlinear components that are the result of a coupling to the quasiradial mode. A corresponding triplet of frequencies was identified in the GW spectrum, when the individual masses of the compact objects are in the most likely range of 1.2 to 1.35 M_{\odot} . A specific frequency peak in the GW spectrum can thus be associated with the nonlinear component resulting from the difference between the $m = 2$ mode and the quasiradial mode. This association is especially strong in the case of hadronic EOSs and could be exploited in the case of future detections, in order to characterize the properties of the post-merger remnant. For this, it will be necessary to obtain accurate frequencies of the quasiradial and quadrupole oscillation modes for a large sample of theoretically possible post-merger remnants and construct empirical relations, depending on a few gross properties, such as the mass and radius of the star. Given the determination of two frequencies and of the total mass of the system from the inspiral signal, these empirical relations could be inverted to yield crucial information on the properties of high-density relativistic objects.

It would further be interesting to test the sensitivity of our results to the spatial conformal flatness approximation employed here, as well as to assess the influence of magnetic fields on the gravitational wave spectrum. The latter effect can be expected to be small for realistic magnetic fields, although there could be a region in the mass vs. magnetic field parameter space in which the effect could be measurable (for recent results, see Giacomazzo et al. (2011)).

ACKNOWLEDGEMENTS

We are indebted to Harry Dimmelmeier and John L. Friedman for useful discussions and to Luciano Rezzolla for useful comments on the manuscript. We thank Stefan Hild for providing the sensitivity curve of the Einstein Telescope and David Shoemaker for providing the Advanced LIGO sensitivity curve and for reading the manuscript. In Garching the project was supported by the Deutsche Forschungsgemeinschaft through the Transregional Collaborative Research Centers SFB/TR 7 “Gravitational Wave Astronomy” and SFB/TR 27 “Neutrinos and Beyond”, and the Cluster of Excellence EXC 153 “Origin and Structure of the Universe” (<http://www.universe-cluster.de>). Computer time grants at the Leibniz-Rechenzentrum München, and the RZG in Garching are acknowledged. This work was supported by CompStar, a Research Networking Programme of the European Science Foundation.

This paper has been typeset from a $\text{\TeX}/\text{\LaTeX}$ file prepared by the author.

REFERENCES

- Abadie J., et al., 2010, *Classical and Quantum Gravity*, 27, 173001
 Abbott B., et al., 2009, *Rept. Prog. Phys.*, 72, 076901
 Abdikamalov E. B., Dimmelmeier H., Rezzolla L., Miller J. C., 2009, *MNRAS*, 392, 52
 Acernese F., et al., 2006, *Class. Quant. Grav.*, 23, S635
 Allen G. D., Andersson N., Kokkotas K. D., Laguna P., Pullin J. A., Ruoff J., 1999, *Phys. Rev. D*, 60, 104021
 Baiotti L., Giacomazzo B., Rezzolla L., 2008, *Phys. Rev. D*, 78, 084033
 Bauswein A., Janka H., Oechslin R., 2010, *Phys. Rev. D*, 82, 084043
 Bauswein A., Oechslin R., Janka H., 2010, *Phys. Rev. D*, 81, 024012
 Belczynski K., O’Shaughnessy R., Kalogera V., Rasio F., Taam R. E., Bulik T., 2008, *Astrophys. J. Lett.*, 680, L129
 Bodmer A. R., 1971, *Phys. Rev. D*, 4, 1601
 Demorest P. B., Pennucci T., Ransom S. M., Roberts M. S. E., Hessels J. W. T., 2010, *Nature*, 467, 1081
 Dimmelmeier H., Bejger M., Haensel P., Zdukaj J. L., 2009, *MNRAS*, 396, 2269
 Duez M. D., 2010, *Classical and Quantum Gravity*, 27, 114002
 Farhi E., Jaffe R. L., 1984, *Phys. Rev.*, D30, 2379
 Gaertig E., Kokkotas K. D., 2011, *Phys. Rev. D*, 83, 064031
 Giacomazzo B., Rezzolla L., Baiotti L., 2011, *Phys. Rev. D*, 83, 044014
 Glendenning N., 1996, *Compact Stars*. Springer-Verlag, New York
 Haensel P., Potekhin A. Y., Yakovlev D. G., 2007, *Neutron Stars 1*. Springer-Verlag, New York
 Harry G. M., the LIGO Scientific Collaboration 2010, *Classical and Quantum Gravity*, 27, 084006
 Hempel M., Schaffner-Bielich J., 2010, *Nuclear Physics A*, 837, 210
 Hild S., Chelkowski S., Freise A., Franc J., Morgado N., Flaminio R., DeSalvo R., 2010, *Classical and Quantum Gravity*, 27, 015003
 Kiuchi K., Sekiguchi Y., Shibata M., Taniguchi K., 2009, *Phys. Rev. D*, 80, 064037
 Lattimer J. M., Prakash M., 2007, *Physics Reports*, 442, 109
 Lattimer J. M., Swesty D. F., 1991, *Nuclear Physics A*, 535, 331
 Oechslin R., Janka H.-T., 2007, *Phys. Rev. Lett.*, 99, 121102
 Oechslin R., Janka H.-T., Marek A., 2007, *Astron. Astrophys.*, 467, 395
 Oechslin R., Rosswog S., Thielemann F.-K., 2002, *Phys. Rev. D*, 65, 103005
 Passamonti A., Stergioulas N., Nagar A., 2007, *Phys. Rev. D*, 75, 084038
 Punturo M., Abernathy M., Acernese F., Allen B., Andersson N., Arun K., Barone F., Barr B., Barsuglia M., Beker M., et al. 2010, *Class. Quant. Grav.*, 27, 084007
 Read J. S., Markakis C., Shibata M., Uryū K., Creighton J. D. E., Friedman J. L., 2009, *Phys. Rev. D*, 79, 124033
 Rezzolla L., Baiotti L., Giacomazzo B., Link D., Font J. A., 2010, *Class. Quant. Grav.*, 27, 114105
 Shen G., Horowitz C. J., O’Connor E., 2011, *ArXiv e-prints*
 Shen G., Horowitz C. J., Teige S., 2010a, *Phys. Rev. C*, 82, 015806
 Shen G., Horowitz C. J., Teige S., 2010b, *Phys. Rev. C*, 82, 045802
 Shen G., Horowitz C. J., Teige S., 2011, *Phys. Rev. C*, 83, 035802
 Shen H., Toki H., Oyamatsu K., Sumiyoshi K., 1998, *Nuclear*

- Physics A, 637, 435
- Shibata M., Taniguchi K., 2006, Phys. Rev. D, 73, 064027
- Shibata M., Taniguchi K., Uryū K., 2005, Phys. Rev. D, 71, 084021
- Shibata M., Uryū K., 2002, Progr. Theoret. Phys., 107, 265
- Steiner A. W., Lattimer J. M., Brown E. F., 2010, Astrophys. & Space Sci., 722, 33
- Stergioulas N., 2003, Living Rev. Relativity, 6, 3
- Stergioulas N., Apostolatos T. A., Font J. A., 2004, MNRAS, 352, 1089
- Thorsett S. E., Chakrabarty D., 1999, ApJ, 512, 288
- Typel S., Röpke G., Klähn T., Blaschke D., Wolter H. H., 2010, Phys. Rev. C, 81, 015803
- Witten E., 1984, Phys. Rev. D, 30, 272
- Zanotti O., Font J. A., Rezzolla L., Montero P. J., 2005, MNRAS, 356, 1371
- Zhang C. M., Wang J., Zhao Y. H., Yin H. X., Song L. M., Menezes D. P., Wickramasinghe D. T., Ferrario L., Chardonnet P., 2010, ArXiv e-prints
- Zhuge X., Centrella J. M., McMillan S. L. W., 1994, Phys. Rev. D, 50, 6247